Sains Malaysiana 53(11)(2024): 3721-3734
http://doi.org/10.17576/jsm-2024-5311-15

Highly Crystalline, Pure ZSM-5 from K_2CO_3-Treated Mud and Its Catalytic Activity in Biodiesel Production

(Tinggi Hablur, ZSM-5 Tulen daripada Lumpur Dirawat K_2CO_3 dan Aktiviti Pemangkinnya dalam Pengeluaran Biodiesel)

HARTATI HARTATI[1,*], QURROTA A'YUNI[1], MEDYA AYUNDA FITRI[2], ADIBA NAILA IZZAH[1], MELINDA INTAN NOVITALINA[1], PUTRI BINTANG DEA FIRDA[1], TAZKIYATUN NUFUS[1], DIDIK PRASETYOKO[3], HARMAMI HARMAMI[3], HASLIZA BAHRUJI[4] & SHAHRUL NIZAM AHMAD[5]

[1]*Department of Chemistry, Faculty of Science and Technology, Universitas Airlangga, Campus C, UNAIR, Mulyorejo, Surabaya, 60115, Indonesia*
[2]*Department of Chemical Engineering, Nahdlatul Ulama University Sidoarjo, Sidoarjo, 61234, Indonesia*
[3]*Department of Chemistry, Faculty of Science and Data Analytics, Institut Teknologi Sepuluh Nopember, Surabaya, 60111, Indonesia*
[4]*Center for Advanced Material and Energy Science, Universiti Brunei Darussalam, Jl. Tungku Link, Gadong BE1410, Brunei*
[5]*School of Chemistry and Environment, Faculty of Applied Sciences, Universiti Teknologi MARA, 40450 Shah Alam, Selangor, Malaysia*

Received: 19 April 2024/Accepted: 27 September 2024

ABSTRACT

Addressing the challenge of clean energy and waste management for sustainable development goals, ZSM-5 were synthesized from high-abundance volcano mud (VM) precursor and then utilized as catalyst in biodiesel production. Unlike conventional alkali treatment, we used the reflux method to extract the silica-alumina from the VM. K_2CO_3 alkali salt was utilized as the extractor, activator, and structure-directing agent. The synthesis was also performed using NaOH as a comparison. Various analytical techniques were employed including XRD, FTIR, SEM-EDX, TEM, N_2 physisorption, and GC-MS to identify the effect of alkali types on the crystallization rate, morphology, and catalytic activity. Highly crystalline, pure ZSM-5 was successfully synthesized. It is found that K_2CO_3 facilitates a slow crystallization rate, requiring a minimum of 5 h of hydrothermal treatment to produce ZSM-5. Interestingly, slow crystallization led to homogeneous ZSM-5 particles with a narrow size distribution and a high mesoporous structure. In contrast, NaOH promoted a faster crystallization rate, producing inhomogeneous ZSM-5 particles size with a dominant microporosity. Two different feedstock qualities i.e., waste cooking oil (WCO) and oleic acid (OA) were used to assess the catalyst's versatility. Among all zeolites synthesized using K_2CO_3, ZK6 exhibited the highest activity, with an 85.9% yield and 30% selectivity for FAME in WCO feedstock. In high-quality OA feedstock, ZK6 achieved significantly higher activity of 97.1% yield with 87.6% selectivity for FAME. ZNa6, the comparable sample synthesized with NaOH, achieved a 78.2% yield with 60.4% FAME selectivity in WCO feedstock. A higher catalytic activity of 97.5% yield with 100% selectivity towards FAME was achieved using high-purity OA feedstock.

Keywords: Biodiesel; K_2CO_3; waste cooking oil; ZSM-5

ABSTRAK

Menangani cabaran tenaga bersih dan pengurusan sisa untuk matlamat pembangunan mampan, ZSM-5 telah disintesis daripada prekursor lumpur gunung berapi (VM) yang memiliki kelimpahan tinggi dan kemudian digunakan sebagai pemangkin dalam pengeluaran biodiesel. Berbeza daripada proses rawatan alkali konvensional, kami menggunakan kaedah refluks untuk mengekstrak alumina silika dalam VM. Garam alkali K_2CO_3 digunakan sebagai pengekstrak, pengaktif, serta agen pengarah struktur. Sintesis juga dilakukan menggunakan NaOH sebagai perbandingan. Pelbagai teknik analisis digunakan contohnya, XRD, FTIR, SEM-EDX, TEM, N_2 fisisorpsi dan GC-MS untuk mengenal pasti kesan jenis alkali ke atas kadar penghabluran, morfologi dan aktiviti pemangkin. ZSM-5 tulen yang sangat kristal telah berjaya disintesis. Didapati bahawa K_2CO_3 memudahkan kadar penghabluran yang perlahan, memerlukan sekurang-kurangnya 5 jam masa hidroterma untuk menghasilkan ZSM-5. Menariknya, penghabluran perlahan membawa kepada zarah ZSM-5 homogen

dengan taburan saiz sempit dan struktur mesoporus yang lebih tinggi berbanding ZSM-5 yang disintesis dengan NaOH. Sebaliknya, NaOH memudahkan kadar penghabluran yang lebih tinggi, menghasilkan saiz zarah ZSM-5 yang tidak homogen dengan struktur mikroporous yang dominan. Dua kualiti bahan mentah yang berbeza iaitu sisa minyak masak (WCO) dan asid oleik (OA) digunakan untuk mengenal pasti kepelbagaian pemangkin. Didapati bahawa antara semua pemangkin yang disintesis dengan K_2CO_3, ZK6 menunjukkan prestasi tertinggi dengan hasil 85.9% dan selektiviti 30% kepada FAME dalam bahan suapan WCO. Manakala dalam bahan suapan OA, ZK6 menunjukkan 97.1% hasil dengan 87.6% selektiviti kepada FAME. ZNa6, sampel setandingnya mencapai hasil 78.2% dengan selektiviti FAME 60.4% dalam bahan suapan WCO. Aktiviti pemangkin yang lebih tinggi sebanyak 97.5% hasil dengan selektiviti 100% terhadap FAME dicapai menggunakan bahan suapan OA ketulenan tinggi.

Kata kunci: Biodiesel; K_2CO_3; sisa minyak masak; ZSM-5

INTRODUCTION

Clean energy sources and waste management are two of the enormous challenges in achieving sustainable development goals. The continuous exploration of fossil fuels raises several concerns, such as depleted reserve and large emissions of greenhouse gasses, which could potentially lead to an energy crisis and global warming. Consequently, researchers are actively developing new, reliable alternative energy sources (Lamnatou, Cristofari & Chemisana 2024; Van Poecke, Tabari & Hellinckx 2024). Biodiesel is deemed a potential substitute for conventional fossil fuels. It is composed of fatty acid alkyl ester (FAAE) and has similar essential fuel properties but with cleaner combustion compared to conventional fossil fuels.

The distinct advantage of biodiesel is that it can be produced from waste materials, employing the circular economy principle to produce renewable energy (Praveena et al. 2024; Sathish Kumar, Sasikumar & Dhilipkumar 2024). Waste cooking oil (WCO) is a potential low-cost feedstock for biodiesel production. Globally, about 18 million tons of waste cooking oil is produced each year (Wan Nur Aifa et al. 2016). Converting WCO to biodiesel not only creates an environmentally friendly renewable fuel but also promotes waste management and sustainable economic growth. However, a key challenge in utilizing WCO for biodiesel production is its high moisture and free fatty acid (FFA) content (Dang, Pham & Dang 2019). Water moisture can lead to the hydrolysis of triglycerides and FAAE, while FFA can trigger saponification when reacting with alkaline catalysts, consequently reducing the biodiesel yield (Chanakaewsomboon et al. 2020).

Acidic catalysts have been proven to be insensitive to saponification of FFA, giving access to biodiesel production from low-quality feedstock via both esterification and transesterification (Guo et al. 2023; Ribeiro et al. 2024; Wu et al. 2024). Despite the high catalytic activity of conventional homogeneous catalysts such as hydrochloric acid, liquid catalysts possess major drawbacks of corrosivity and the need for tedious neutralization, separation, and purification steps (Guldhe et al. 2017; Su 2013). Heterogeneous acid catalysts have been widely adopted as substitutes for homogeneous catalysts due to their advantageous properties, including ease of recovery, high reusability, and environmentaly friendliness (Ye et al. 2024; Zhang et al. 2019). Furthermore, their unique structural and textural properties remarkably promote its catalytic activity, selectivity, and stability (Weckhuysen & Wachs 2001).

Numerous types of solid acid catalysts such as zeolites (Kowalska-Kuś et al. 2024), metal-organic framework (MOF) (Yang et al. 2023), alumina (Ponce et al. 2024), and sulfonated carbon (Hadeer et al. 2023) have been employed in biodiesel production. Zeolites offer unique properties of tunable Brönsted and Lewis acidity, which can lead to favorable synergistic effects in biodiesel production (Araújo Silva et al. 2020; Mao et al. 2023). ZSM-5 is classified as highly acidic zeolite, attributed to its high Si/Al ratio (Gomes, Zalazar & Arroyo 2022). Previous studies have reported the superior performance of ZSM-5 catalysts in biodiesel production. Sulfonated hierarchical ZSM-5 (SO_3H-H-ZSM-5) has shown a 92.45% yield of methyl ester in the esterification of oleic acid (Nermein et al. 2021). Through a different reaction pathway, a comparative study showed that H-ZSM-5 exhibited the highest liquid yield of biofuel compared to HY and Al_2O_3 catalysts (Rajasree et al. 2024).

Although commercially available, zeolites are still widely synthesized on a laboratory scale to incorporate specific and desirable properties for high catalytic activities. Generally, ZSM-5 is synthesized from chemical reagents such as sodium aluminate and silica colloidal as aluminum and silicon sources (Rezayan & Taghizadeh 2018). The increasing environmental concerns have raised the urge to develop greener pathways in zeolite synthesis by utilizing highly abundant natural materials such as clay and mud (Hartati et al. 2020; Novita et al. 2022). Volcano mud is a type of mud produced from subsurface geothermal activity, where fractures or fault zones trigger its eruption onto the Earth's surface (Schulze-Makuch et al. 2020). Volcano mud located in Sidoarjo, Indonesia, is reported to have high silica and moderate alumina content

(Qurrota et al. 2023), making it a potential source of silica alumina for zeolite synthesis. However, the diverse impurities present in volcano mud make it challenging to extract high-puritiy silica and alumina compounds. A previous study reported the successful synthesis of Y zeolite from volcano mud through an acid leaching- alkali smelting pretreatment process using HCl and NaOH, respectively (Novita et al. 2022). Sodium hydroxide (NaOH) is widely used in zeolite synthesis. The hydroxide ions act as a mineralizing agent, enhancing the solubility of silica and alumina species (Grand, Awala & Mintova 2016). Another potential reagent is potassium carbonate (K_2CO_3), a mild base that has not been intensively explored compared to NaOH in zeolite synthesis. A previous study demonstrated the effective silica-alumina extraction from leached illite through an alkali fusion process process using K_2CO_3 (Li et al. 2021), suggesting its promising use in zeolite synthesis.

In this paper, a greener approach to the synthesis of ZSM-5 catalysts was employed by utilizing high-abundance volcano mud as the precursor. It is worth noting that for the first time, the conventional alkaline treatment was done through the reflux methodwith K_2CO_3 as the extractor and activator. The synthesis was then carried out through hydrothermal method with different reaction times of 3, 5, and 6 h. The synthesized catalysts were used for biodiesel production from WCO and OA. As comparison samples, three ZSM-5 catalysts were prepared tusing the same method, but utilizing NaOH for the alkaline treatment process. Further investigations were conducted to study the effect of K_2CO_3 on the ZSM-5 crystal growth, morphology, and catalytic activity in biodiesel production. X-ray diffraction (XRD) was employed to study the phase transformation and crystal growth. The chemical bonds of the catalysts and catalysts acidity were analyzed using Fourier transform infrared (FTIR). The effect of the alkali type and synthesis condition on the morphology and textural properties of the synthesized catalysts was identified through scanning electron microscope- energy dispersive X-rays (SEM-EDX), transmission electron microscopy (TEM), and nitrogen isotherm physisorption. The biodiesel content in the products of the catalytic reaction was analyzed using gas chromatography-mass spectroscopy (GC-MS).

MATERIALS AND METHODS

REAGENTS

The volcano mud (VM) sample was taken from Sidoarjo, Indonesia. Waste cooking oil was collected from household waste in Surabaya. Potassium carbonate (K_2CO_3, ≥99%, Merck), hydrochloric acid (HCl, 37%, Merck), sodium hydroxide (NaOH, 99%, Merck), tetrapropylammonium hydroxide (TPAOH, 40 wt%, Merck), silica colloidal (LUDOX®, 40 wt%, Aldrich), ammonium acetate (CH_3COONH_4, 98%, Merck), methanol (anhydrous, 99.8%, Aldrich), oleic acid ($CH_3(CH_2)_7CH{=}CH(CH_2)_7COOH$, 65-88%, Fluka), were used as received. In-lab-produced deionized (DI) water was used for the experiment.

PRE-TREATMENT OF VOLCANO MUD

VM was grounded, washed, and dried in the oven at 100 °C for 24 h. The powder was sieved using 140-mesh sieves before being mixed with HCl 1M (1:5 weight to volume). The mixture was heated at 60 °C and continuously stirred for 2 h, referred to as the acid-leaching process. The successful removal of t metal oxides can be seen in the resulting brown-yellowish filtrate, indicating the dissolution of Fe_2O_3(s) by HCl forming $FeCl_3$(aq). The solid was collected, washed with DI water until the pH was neutral, then dried at 100 °C for 24 h. It was subsequently calcined at 680 °C for 1 h and labeled as leached VM (LVM). The silica and alumina in the LVM were then extracted and activated through alkaline treatment. LVM was mixed with alkali (K_2CO_3 or NaOH) 2 M in a 1:10 weight-to-volume ratio and refluxed at 90 °C for 1 h. The filtrate was collected and used directly as a precursor in ZSM-5 synthesis. To identify the composition of the filtrate, it was transformed into xerogel by mixing with 1 M HCl until the pH reached 8. The resulting xerogel was aged overnight and then oven-dried at 80 °C for 18 h. The composition of the dried xerogel was then analyzed using an X-ray fluorescence (XRF) spectrometer.

CATALYSTS SYNTHESIS

ZSM-5 was synthesized by mixing VM filtrate as the silica-alumina source, TPAOH as the structure-directing agent, LUDOX® as an additional silica source, and DI water with a mol ratio of 1 SiO_2: 0.0065 Al_2O_3: 0.06111 TPAOH:38 H_2O. The mixture formed a colloidal gel, which was then aged in continuous stirring for 24 h. The aged mixture was transferred to a Teflon-lined autoclave and heated in an oven at 190 °C for 3, 5, and 6 h of reaction time. After cooling to room temperature, the mixture was washed with DI water until neutral pH. The collected solid was then dried in an oven at 100 °C for 24 h, followed by calcination at 550 °C for 6 h. Catalysts prepared from K_2CO_3-treated VM are annotated as ZKx, whereas catalysts prepared from NaOH-treated VM are annotated as ZNax, here x denotes the duration of the hydrothermal reaction. For example, ZNa3 is prepared from NaOH-extracted VM with a 3 h hydrothermal reaction. The as-prepared catalysts were activated through a cation exchange process before the catalytic reactions. Weighed 1 g of catalyst was mixed with 50 mL ammonium acetate solution 0.5 M and refluxed at 60 °C for 3 h. The mixture was then washed with DI water,dried at 100 °C for 24 h, and calcined at 550 °C for 5 h.

CHARACTERIZATION OF CATALYSTS

The phase transformation and crystal growth of the sample were analyzed using an X-ray diffractometer (XRD) Philips X-pert MPD-1. Further analysis was done by calculating the crystallite size of the samples according to the Scherrer equation:

$$Dc = \frac{K\lambda}{(\beta \cos\theta)}$$

where Dc is crystallite size; K is the Scherrer constant; λ is the wavelength of the Cu X-ray source; β is full width at half maximum (FWHM, in radians); and θ is diffraction angle (Md Sahabat et al. 2023).

The composition of the sample was identified using X-ray fluorescence (XRF) spectrometer Philips Panalytical Minipal 4. The chemical bonds were characterized with a Fourier transform infrared (FTIR) spectrometer Shimadzu IR Tracer-100. The morphology of the samples was observed using a scanning electron microscope (SEM), and energy dispersive X-rays (EDX) elemental mapping was performed using a Hitachi FlexSEM 100 II. The textural properties of the sample were analyzed by N_2 physisorption using an Autosorb iQ Station 1. Transmission electron microscopy (TEM) analysis was conducted using a Tecnai G2 20S transmission electron microscope.

BIOFUEL PRODUCTION

The catalytic activity of ZSM-5 was evaluated for biofuel production from WCO and OA. The cation-exchanged catalyst was heated in an oven at 100 °C for 24 prior to the reaction. Then, 0.25 g of the catalyst was mixed with 5 mL of waste cooking oil and 20 mL of methanol in a round-bottom flask. The mixture was refluxed at 65 °C with continuous stirring at 500 rpm for 2 h (Devaraj Naik & Udayakumar 2019). Afterward, the mixture was filtrated through the filter paper. The collected filtrate was mixed with 10 mL of n-hexane in a separation funnel to extract the reaction product. The upper layer contains the extracted product in the n-hexane phase. The product was then isolated by evaporating the n-hexane. To further study the effect of feedstock quality on the reaction pathway and product in biofuel production, a similar reaction was done using oleic acid as the feedstock according to the reported literature (Modather et al. 2021).

FREE FATTY ACID (FFA) TEST

The effectiveness of the esterification process is determined by the conversion of FFA. The FFA content in the waste cooking oil feedstock was measured using the titration method (Medeiros Vicentini-Polette et al. 2021). Weighed 2.82 g of waste cooking oil was dissolved in 5 mL ethanol, then mixed with 3 drops of 2% phenolphthalein indicator. The mixture was titrated with 0.013 N NaOH until the color changed from yellowish to pinkish. The free fatty acid content was then calculated using the following equation:

$$\text{FFA}(\%) = \frac{(V.N.A)}{m} \times 100\%$$

where V is the volume of NaOH used in the titration; N is the normality of NaOH solution; A is the molecular weight of the FFA; and m is the weight of the sample (Medeiros Vicentini-Polette et al. 2021).

WATER CONTENT ANALYSIS

The water content of the waste cooking oil was analyzed using the gravimetry method. Weighed 2 g of waste cooking oil (m_i) was put in the container with a known mass andheated in the oven at 110 °C for 24 h. The dried sample and the container was then weighed (m_f). The heating-weighing process was repeated a until a constant m_f value was obtained. The water content was calculated using the following equation (Bilskie 2001):

$$\text{Water content}(\%) = \frac{m_i - m_f}{m_f} \text{ x } 100$$

GC-MS ANALYSIS

Liquid products from the catalytic reaction were analyzed using a gas chromatography-mass spectrometer (GC-MS) Agilent 7890 B with an HP-5MS column. The analysis was performed with under following conditions: An initial temperature of 60 °C, a first heating rate of 10 °C/min to 150 °C, and a second heating rate of 5 °C/min to 250 °C. The peak area from the GC spectrum was used to calculate the yield of products, whereas the MS spectrum was used to identify chemical compounds in the liquid products. The percentage of liquid yield was determined using the following equation (Yadav, Yadav & Ahmaruzzaman 2023):

$$\text{Yield}(\%) = \frac{(\text{weight of liquid product})}{(\text{weight of feedstock})} \text{ x } 100\ \%$$

The selectivity of the product was calculated using the following equation (Trisunaryanti et al. 2020):

$$\text{Product selectivity}(\%) = \frac{(\text{peak area of desired product})}{(\text{peak area of total product})} \text{ x } 100\ \%$$

RESULTS AND DISCUSSION

EFFECT OF K_2CO_3 ALKALI SALT TREATMENT ON THE GROWTH AND SIZE OF ZSM-5 CRYSTAL

High silica extraction from the VM was confirmed from the XRF analysis of the resulting xerogel, as summarized in Table 1. The xerogel contains 71.5% and 86.3% SiO_2 for K_2CO_3 and NaOH treatment, respectively. Moreover, the low content of alumina (2-10%) in both xerogel is preferable for the synthesis of silica-rich ZSM-5. Figure 1. A. shows the diffractogram of the VM precursor and treated VM. The diffractogram of VM shows a highly crystalline quartz (SiO_2) peak at 2θ of 26.55°, with low-intensity alumina at 2θ around 30-40° (JCPDS no 00-006-0221 and 86-1410). After the alkali treatment process, the diffractogram showed a hump broad peak around 20-25°, indicating the amorphous phase of the xerogels (Zhang, Li & Zhang 2019). Two small peaks at ~29° and ~40° are observed from XK, indicating traces of crystalline impurities phase in xerogel, presumably due to the slower dissolution reaction by K_2CO_3 compared to NaOH. Upon the alkali treatment process, the crystalline silica-alumina in the VM was transformed into a highly active amorphous silica-alumina phase. This result demonstrates the successful extraction and activation of VM.

Figure 1(B) shows the diffractogram of the synthesized catalysts. After 3 h of hydrothermal reaction, ZK3 exhibits a broadened peak around 20-25° with small intensity peaks around 7.8°, 9.4°, and 24.3°, showing an amorphous aluminosilicate phase with the initial growth of ZSM-5. In contrast, ZNa3 exhibits the characteristic peaks of ZSM-5 at 7.8°, 9.4°, 12.8°, 20.8°, 23.1°, 23.6°, 24.3°, 25.6°, 26.6°, and 28.6° (JCPDS no 44-003). This result suggests a slower crystallization rate for the synthesis with the K_2CO_3-extracted precursor. There are several factors affecting the alkali treatment process, including basicity, gel viscosity, affinity to H_2O, and cation size (Prodinger et al. 2023). XRF analysis showed a total of 18.5% impurities present in K_2CO_3-treated xerogel. These impurities might hinder the polycondensation process, leading to a longer ZSM-5 crystallization time. In contrast, higher purity of silica-alumina obtained from NaOH-treated xerogel led to higher encounters between precursors, acceleraing the nucleation and polycondensation, and facilitating faster crystallization.

Prolonged hydrothermal reaction of 5 and 6 h shows a diffractogram pattern of ZSM-5 with increased intensity. Samples ZK5, ZK6, ZNa5, and ZNa6 showed similar diffraction patterns with indications of highly crystalline and pure ZSM-5. Further analysis of the diffractogram was done by calculating the crystallite size based on the Scherrer equation. ZK5 and ZK6 which prepared through K_2CO_3 treatment have slightly larger crystallite size of 90.7 nm and 93.9 nm, respectively. ZNa3, ZNa5, and ZNa6 which prepared through NaOH treatment have slightly smaler crystallite size of 84.4 nm, 27 nm, and 41 nm, respectively. This phenomenon is attributed to the slower crystallization facilitated by potassium cation which led to the formation of large crystals, contrary, the fast crystallization process facilitated by sodium cation led to the formation of small crystals (Jonscher et al. 2022; Liu et al. 2014).

FTIR STUDY

The FTIR spectra of the synthesized samples are depicted in Figure 2. All samples exhibit similar absorption bands at ~1000 cm^{-1} attributed to the asymmetric stretching of Si-O-Si or Si-O-Al bonds, while absorption bands at ~1200 cm^{-1} and ~800 cm^{-1} are due to symmetric stretching of Si-O-Al bonds (Lønstad Bleken et al. 2013). The characteristic bands of the five-membered ring in ZSM-5 appear at ~550 cm^{-1} for all samples except ZK3 (Amalia et al. 2017). This result is consistent with the XRD analysis which showed that ZK3 is amorphous aluminosilicate. The absorption band at a lower wavenumber of ~450 cm^{-1} is attributed to the bending vibrations of Si-O and Al-O bonds.

EFFECT OF K_2CO_3 ALKALI SALT TREATMENT IN ZSM-5 CRYSTALS MORPHOLOGY AND PARTICLE SIZE DISTRIBUTION

Zeolite morphology affects its catalytic activity, selectivity, and stability. The morphology of the synthesized samples, observed from SEM images, is depicted in Figure 3. Consistent with the XRD analysis, the SEM image of ZK3 showed non-uniform particle chunks, suggesting the amorphous phase of the sample. In contrast, ZNa3 exhibits oval prism crystals of ZSM5. The effect of alkali type in the ZSM-5 crystal morphology is clearly shown by samples synthesized in prolonged hydrothermal time of 5 and 6 h. Sample ZK5 and ZK6 which synthesized with K_2CO_3 showed hexagonal prism morphology with dull edges due to the convex sides. In contrast, both ZNa5 and ZNa6 exhibit highly crystalline hexagonal prism crystals with well-defined edges and slightly longer c-axis lengths. The longer c-axis length in this sample implies the preferential facet growth along the c-axis, resulting in a longer diffusion path for the sinusoidal channels inside the ZSM-5 crystals (Dai et al. 2021).

Samples synthesized with NaOH treatment show homogeneous particle size at the 3-hour reaction time (ZNa3). However, a broader particle size distribution is observed withprolonged 5 and 6 of hydrothermal time. SEM images of ZNa5 and ZNa6 shows significantly larger ZSM-5 particles. Interestingly, ZK5 and ZK6 average particle size increase from 1.72 to 2.43 μm, but the homogeneity remains unchanged with the increase of reaction time. A trend of increasing particle size with synthesis time is

TABLE 1. Chemical composition of VM and xerogel

Compound (%)	VM	K_2CO_3 xerogel	NaOH xerogel
SiO_2	48.1	71.5	86.3
Al_2O_3	12.0	2[#]	10.0
Fe_2O_3	25.1	0.4	0.3
CaO	6.3	5.1	0.7
K_2O	2.7	1.8	0.7
TiO_2	1.9	-	-
SO_3	1.9	0.6	-
Others*	2.1	10.6	2.1

*Other compounds (CuO, MnO, ZnO, and ZrO_2) in trace amount
[#]Obtained from EDX

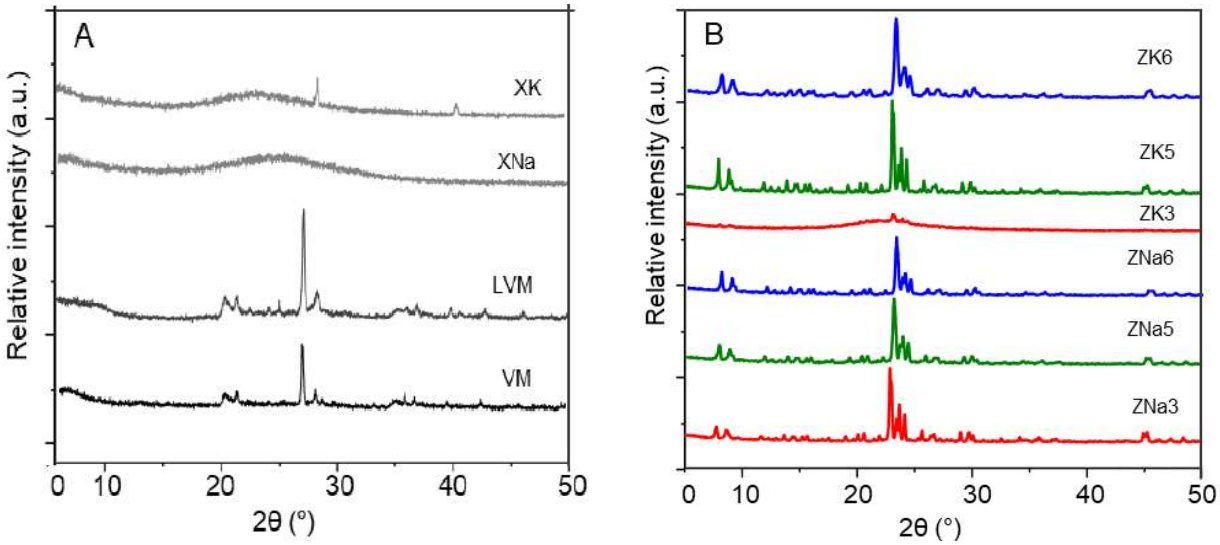

FIGURE 1. XRD analysis of raw volcano mud (VM), acid-leached VM (LVM), xerogel extracted from NaOH (XNa), and xerogel extracted using K_2CO_3 (XK)(A), and the synthesized catalysts (B)

attributed to the aluminium zoning in the crystal (Li et al. 2020). The fast crystallization rate facilitated by NaOH might led to premature crystallization, producing ZSM-5 particles with significant size variations. The result suggest that the slower crystallization rate facilitated by K_2CO_3 is preferable for producing crystals with a narrower particle size distribution.

It is worth noting that aside from the typical ZSM-5 crystals, intergrowth crystals of ZSM-5 are present in the ZK5, ZK6, ZNa3, ZNa5, and ZNa6. These intergrowth crystals, known as mortise-tenon ZSM-5 or twinning ZSM-5, form when ZSM-5 crystals make contact on the (010) surface. Further interactions between crystals connect the straight and sinusoidal channels, leading to the 90° intergrown structure (Wang et al. 2022). TEM images of ZK5 depicted in Figure 4. showed the hexagonal crystal of ZSM-5 with lighter intensity around the edges, indicating the presence of a mesoporous structure (Diaz & Mayoral 2011). The darker intensity observed in the center of the crystal is attributed to the intergrowth crystal structure, as observed in the SEM image. The lattice spacing was determined to be ~1 nm, consistent with the reported values (Bloom & Van Reenen 2013; Kulkarni et al. 1982).

TEXTURAL PROPERTIES OF THE SYNTHESIZED CATALYSTS

The isotherm curves of the synthesized catalysts are depicted in Figure 5(A). All isotherm curves showed a hysteresis loop, which is attributed to the condensation process inside the capillaries of the mesoporous structure (Thommes 2010). Due to its amorphous phase, ZK3 has the lowest porosity compared to other catalysts. As summarized

in Table 2, ZK3 exhibits a total micro-mesoporous surface area of 22.9 m^2/g and a total pore volume of 0.02 cc/g. The isotherm curve of ZK6 shows an adsorption range of 65 –105 cc/g, with two inflection points in the desorption curve at P/P_0 0.15 and 0.5, corresponding to hysteresis types H1 and H2.

A noticeable difference is observed in the isotherm curve of ZK5, which has an adsorption volume four times higher than the other samples. A closer look at the adsorption curve shows a distinct increase of ~50-60 cc/g at P/P_0 ~0.15 and a significant increase of ~100-400 cc/g at P/P_0 ~0.9-1.0. The desorption curve also showed inflection points at P/P_0 ~1.0, 0.5, and 0.15. According to the shape of the hysteresis, the curve showed the combination of several hysteresis types: H3 at P/P_0 0.09-0.12, H4 at P/P_0 0.2-0.45, H2 at P/P_0 0.45-0.9, and H1 at P/P_0 ~1.0. According to the IUPAC classification, H1 corresponds to cylindrical pores, H2 to bottleneck-shaped pores, H3 toparallel plate-shaped pores, and H4 to slit-wedge-shaped pores (Wang et al. 2020; Xu et al. 2020).

Samples ZNa3, ZNa5, and ZNa6 exhibit similar isotherm curve types VI, indicating that adsorption happened in two steps. These samples showed similar inflection points and hysteresis types as ZK6 but different adsorption ranges. Both ZNa3 and ZNa6 showed similar adsorption volume ranges of ~70–115 cc/g, whereas ZNa5 shows slightly higher adsorption up to ~140 cc/g. Moreover, ZNa5 has a distinct smaller H2 loops compared to ZNa3, ZNa6, and ZK6.

The multistep isotherm curve observed in all samples indicates that the samples have a multimodal mesoporous structure (Reber & Brühwiler 2015). Further analysis using density functional theory (DFT) calculations, depicted in Figure 5(B), confirms the multimodal mesopore structures. All samples show multiple peaks, primarily within the 2–5 nm pore diameter range. In contrast, a distinct broad peak at a higher pore diameter range of 10–50 nm shown in sample ZK5.

The textural properties of the catalysts, summarized in Table 2, showed that ZSM-5 synthesized with K_2CO_3 has a high mesoporous surface area of 86.1 and 45.8 m^2/g for ZK5 and ZK6, respectively. Interestingly, ZSM-5 synthesized with NaOH has a lower mesoporous surface area of 37.2, 35.5, and 28.1 m^2/g for ZNa3, ZNa5, and ZNa6, respectively. Despite its moderate total pore surface area, ZK5 has the highest total pore volume of 117 cc/g, which is ~10 times higher than the other samples. The high mesopore volume is attributed to the larger mesopore diameter, as shown in Figure 5(B). The high micropore volume is presumably due to the pore shape and connectivity, as indicated by the hysteresis shape in its isotherm curve (Figure 5(A)).

EFFECT OF FEEDSTOCK TYPE ON THE REACTION PATHWAY

The catalytic activity of the catalysts was evaluated in the transformation of WCO into biodiesel. Figure 6(A) shows that among K_2CO_3-treated samples, the highest yield of 85.9% with 30% FAME selectivity was shown by ZK6. ZNa6 as the comparable sample showed lower yield of 78.2% with 60.4% FAME selectivity. Other than FAME as the main product of the esterification, FAAE is also present as the main product in ZK3, ZK5, and ZNa3 catalyzed reactions. This result indicates that both esterification and transesterification happened simultaneously during the reaction. GCMS analysis of WCO showed that the FFA contents in WCO are around ~70%, whereas the ~30% is the mixture of glycidyl palmitate (FAME) and squalene. Triglycerides and FAME in the WCO feedstock undergoes transesterification during biofuel production (Mosharof et al. 2021).

To identify the performance of the synthesized catalysts with different quality feedstocks, high-purity OA was used. According to the product specification sheet, OA contains up to 88% oleic acid, with the rest 12% being a mixture of other fatty acids such as palmitic acid, and stearic acid. As shown in Figure 6(B), the product yield and selectivity significantly enhanced when high-quality feedstock was used. Liquid yield of 87-97.5% were obtained from the conversion of OA with all catalysts, with ZNa6 achieving the highest conversion of 97.5%, followed by ZK6 with 97.1%. Moreover, high FAME selectivity of 87.6-100% was obtained from all catalysts.

The possible reaction pathways in both WCO and OA is shown in Figure 6(C). The low yield of FAME obtained using WCO feedstock can be attributed to the triglyceride content, which undergoes transesterification, producing glycerol byproduct (Pirzadi & Meshkani 2022). Further analysis showed that low-quality feedstock of WCO exhibits undesirable properties of 1.09% FFA and 0.49% water content. Considering the acidic nature of the synthesized catalyst, high FFA content would not lead to saponification. However, the presence of water in oil feedstock can lead to side reactions, such as hydrolysis of glycidyl palmitate to produce dihydroxy alkyl ester (Dorado, Herrerías & Fraile 2023).

Considering the catalytic performance in both WCO and OA feedstock, ZK6 exhibits the highest performance among samples synthesized with K_2CO_3. Despite the low-quality feedstock and possible side reaction pathways, ZK6 achieved a high product yield of 85.9% but a low selectivity of 30% towards FAME. Its comparable sample, ZNa6, which was synthesized with NaOH, achieved a slightly lower yield of 78.2% with a higher FAME selectivity of 60.4%. In high-purity OA feedstock, ZK6 achieved a high product yield of 97.1% with 87.6% FAME selectivity. ZNa6 exhibits slightly higher performance with 97.5% product yield and 100% selectivity towards FAME.

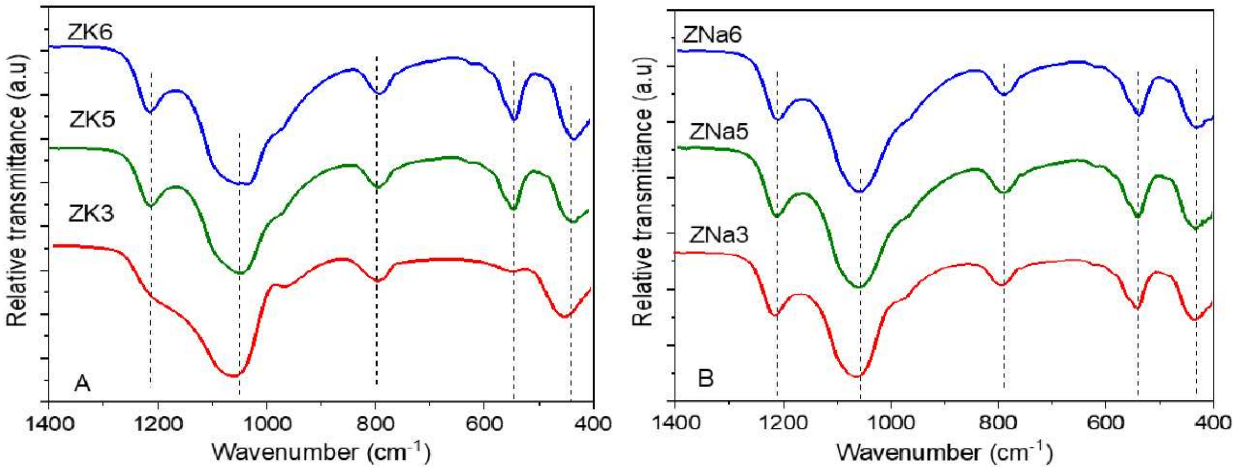

FIGURE 2. FTIR spectra of the samples synthesized with K_2CO_3 (A), and samples synthesized with NaOH (B)

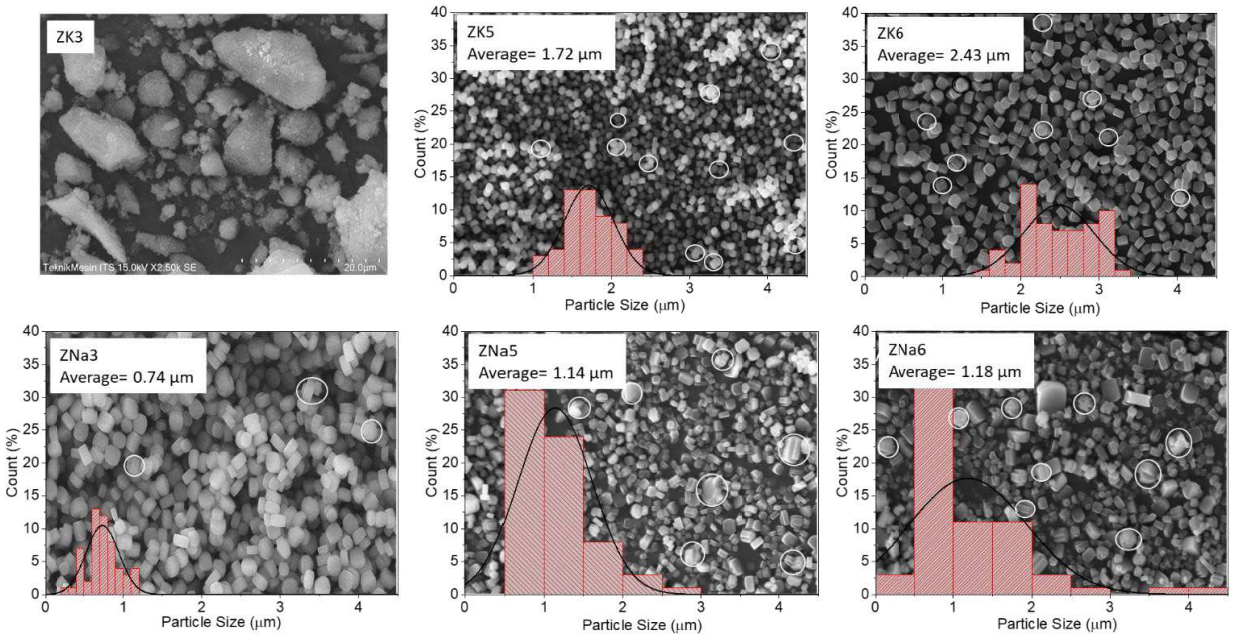

FIGURE 3. SEM images of the synthesized samples, sample ZK3-ZK6 has a magnification of 2.5k times, whereas samples ZNa3- ZNa6 have a magnification of 5k times. White circles indicate intergrowth ZSM-5

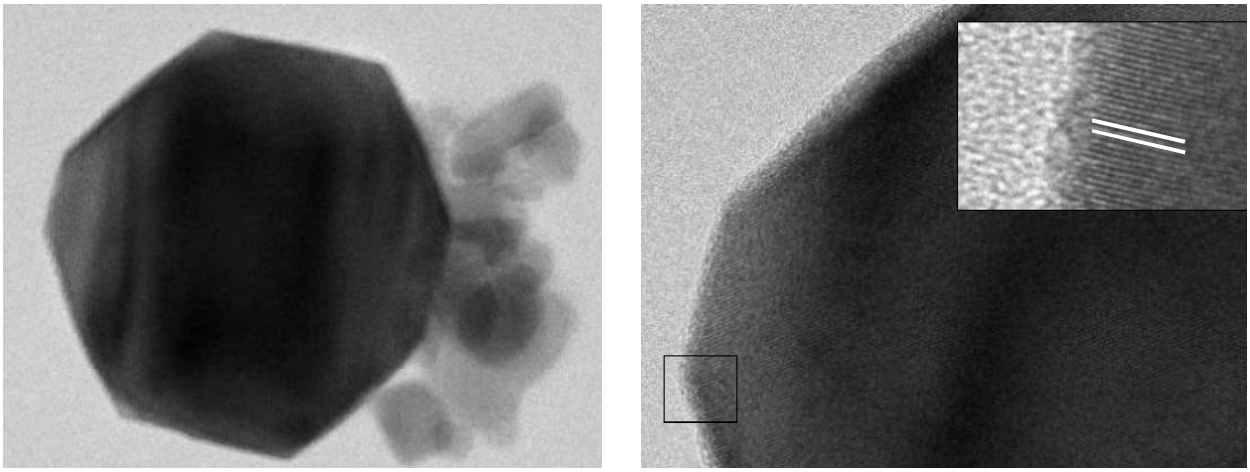

FIGURE 4. TEM images of ZK5 sample

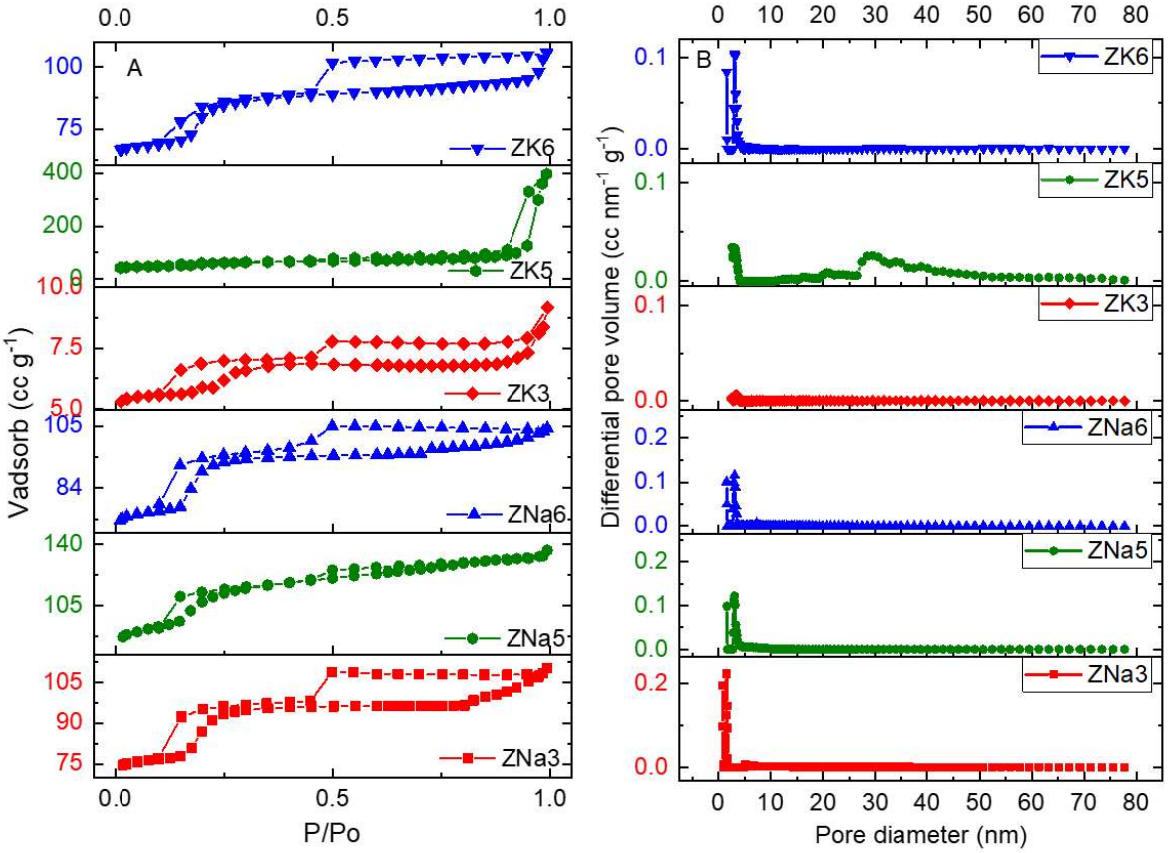

FIGURE 5. Nitrogen adsorption-desorption isotherm of the synthesized samples (A), DFT pore size distribution graph of the synthesized samples, (B)

TABLE 2. Properties of the synthesized catalyst

Code	Si/Al[a]	Mesopore surface area[b] (m^2/g)	Micropore surface area[c] (m^2/g)	Mesopore volume[b] (cc/g)	Micropore volume [c]	Mesopore size[b] (nm)
ZK3	12	2.53	20.39	0.01	0.02	3.81
ZK5	38	86.11	198.37	0.56	0.61	3.81
ZK6	37	45.83	269.31	0.05	0.16	3.82
ZNa3	33	37.15	357.43	0.04	0.17	3.81
ZNa5	27	35.46	357.43	0.05	0.21	3.82
ZNa6	41	28.12	293.80	0.03	0.16	3.82

a. EDX b. BJH c. BET

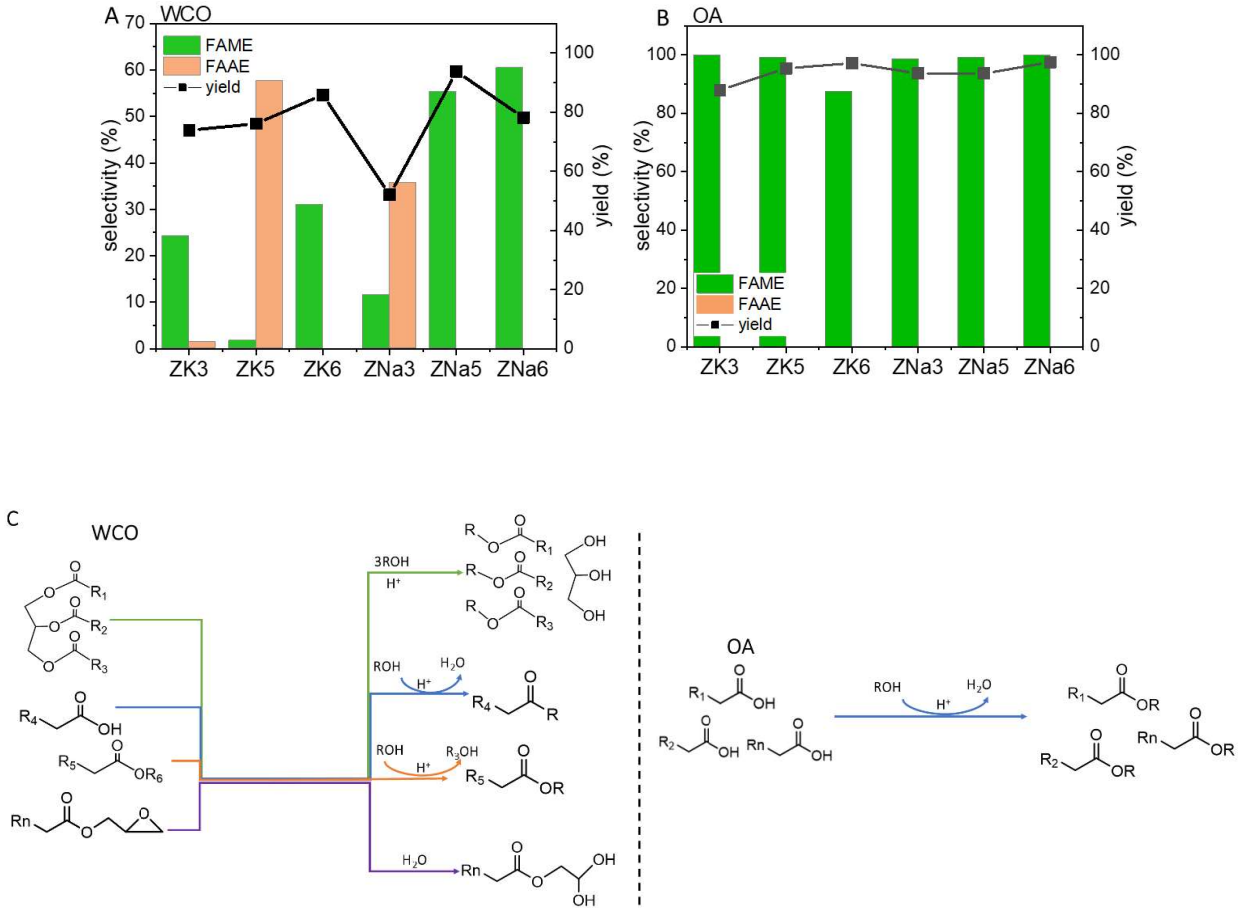

FIGURE 6. Liquid yield and product selectivity of the reactions with WCO (A), and OA (B) feedstock, and its possible reaction pathways (C)

CONCLUSION

A greener approach in biodiesel production was performed by utilizing abundant natural resources as catalyst precursors and waste feedstock. Volcano mud was hydrothermally transformed into a ZSM-5 catalyst through a modified conventional alkali treatment process. The use of alkaline salt K_2CO_3 in the pretreatment process facilitated a slow crystallization rate, resulting in a desirable narrow particle size distribution and higher mesoporous structure. In contrast, NaOH facilitated fast crystallization, produces wide particle size distribution and dominant microporous structure. Among catalysts synthesized with K_2CO_3, catalyst ZK6 exhibits the highest performance with 85.9% yield and 30% selectivity to FAME in low-quality WCO feedstock. In high-purity OA feedstock, ZK6 exhibits 97.1% yield with 87.6% selectivity to FAME. Its NaOH-synthesized counterpart, ZNa6, exhibited a lower 78.2% yield in WCO feedstock but higher higher FAME selectivity of 60.4%. In OA feedstock, ZNa6 exhibited a 97.5% yield with 100% selectivity towards FAME.

ACKNOWLEDGMENTS

The research fund is supported by The Directorate General of Higher Education, Research, and Technology of the Ministry of Education, Culture, Research, and Technology of the Republic of Indonesia, under the research project of Penelitian Kerjasama Dalam Negeri (PKDN) 2023 No: 1294/UN3.LPPM/PT.01.03/2023.

REFERENCES

Amalia Putri Purnamasari, Meyga Evi Ferama Sari, Desy Tri Kusumaningtyas, S. Suprapto, Abdul Hamid & Didik Prasetyoko. 2017. The effect of mesoporous H-ZSM-5 crystallinity as a CaO support on the transesterification of used cooking oil. *Bulletin of Ch44emical Reaction Engineering & Catalysis* 12(3): 329-336. https://doi.org/10.9767/bcrec.12.3.802.329-336

Araújo Silva, D.S., Castelblanco, W.N., Piva, D.H., de Macedo, V., Carvalho, K.T.G. & Urquieta-González, E.A. 2020. Tuning the Brønsted and Lewis acid nature in HZSM-5 Zeolites by the generation of intracrystalline mesoporosity - Catalytic behavior for the acylation of anisole. *Molecular Catalysis* 492: 111026. https://doi.org/10.1016/j.mcat. 2020.111026

Bilskie, J. 2001. Soil water status: Content and potential. *Campbell Scientific* 1784(435): 84321.

Bloom, N. & Van Reenen, J. 2013. Synthesis of zeolite ZSM-5, reaction mixture therefor and product thereof. *NBER Working Papers*.

Chanakaewsomboon, I., Tongurai, C., Photaworn, S., Kungsanant, S. & Nikhom, R. 2020. Investigation of saponification mechanisms in biodiesel production: Microscopic visualization of the effects of FFA, water and the amount of alkaline catalyst. *Journal of Environmental Chemical Engineering* 8(2): 103538. https://doi.org/10.1016/j.jece.2019.103538

Dai, W., Kouvatas, C., Tai, W., Wu, G., Guan, N., Li, L. & Valtchev, V. 2021. Platelike MFI crystals with controlled crystal faces aspect ratio. *Journal of the American Chemical Society* 143(4): 1993-2004. https://doi.org/10.1021/jacs.0c11784

Dang Nguyen Thoai, Pham Thi Le Hang & Dang Thi Lan. 2019. Pre-treatment of waste cooking oil with high free fatty acids content for biodiesel production: An optimization study via response surface methodology. *Vietnam Journal of Chemistry* 57(5): 568-573.

Devaraj Naik, B. & Udayakumar, M. 2019. Optimization studies on esterification of waste cooking oil using sulfated montmorillonite clay acidic catalyst. *Materials Today: Proceedings* 46(Part 19): 9855-9861. https://doi.org/10.1016/j.matpr.2020.11.419

Diaz, I. & Mayoral, A. 2011. TEM studies of zeolites and ordered mesoporous materials. *Micron* 42(5): 512-527. https://doi.org/10.1016/j.micron.2010.12.005

Dorado, V., Herrerías, C.I. & Fraile, J.M. 2023. Catalytic hydrolysis of epoxyfatty esters with solid sulfonic acids. *Molecular Catalysis* 547: 113282. https://doi.org/10.1016/j.mcat.2023.113282

Gomes, G.J., Zalazar, M.F. & Arroyo, P.A. 2022. New insights into the effect of the zeolites framework topology on the esterification reactions: A comparative study from experiments and theoretical calculations. *Topics in Catalysis* 65(7-8): 871-886. https://doi.org/10.1007/s11244-022-01606-5

Grand, J., Awala, H. & Mintova, S. 2016. Mechanism of zeolites crystal growth: New findings and open questions. *CrystEngComm* 18(5): 650-664. https://doi.org/10.1039/c5ce02286j

Guldhe, A., Singh, P., Ansari, F.A., Singh, B. & Bux, F. 2017. Biodiesel synthesis from microalgal lipids using tungstated zirconia as a heterogeneous acid catalyst and its comparison with homogeneous acid and enzyme catalysts. *Fuel* 187: 180-188. https://doi.org/10.1016/j.fuel.2016.09.053

Guo, Y., Delbari, S.A., Namini, A.S., Van Le, Q., Park, J.Y., Kim, D., Varma, R.S., Jang, H.W., T-Raissi, A., Shokouhimehr, M. & Li, C. 2023. Recent developments in solid acid catalysts for biodiesel production. *Molecular Catalysis* 547: 113362. https://doi.org/10.1016/j.mcat.2023.113362

Hadeer S. El Saey, Ahmed O. Abo EL Naga, Mohamed El Saied, Seham A. Shaban, Soha A. Abdel-Gawad & S.A. Salih. 2023. Kinetic and thermodynamic studies on the esterification of oleic acid with methanol over sulfonated biochar catalyst derived from waste tea dregs. *Biomass and Bioenergy* 176: 106892. https://doi.org/10.1016/j.biombioe.2023.106892

Hartati, Wega Trisunaryanti, Rino Rakhmata Mukti, Ika Amalia Kartika, Putri Bintang Dea Firda, Satriyo Dibyo Sumbogo, Didik Prasetyoko & Hasliza Bahruji. 2020. Highly selective hierarchical ZSM-5 from kaolin for catalytic cracking of *Calophyllum inophyllum* oil to biofuel. *Journal of the Energy Institute* 93(6): 2238-2246. https://doi.org/10.1016/j.joei.2020.06.006

Jonscher, C., Seifert, M., Kretzschmar, N., Marschall, M.S., Le Anh, M., Doert, T., Busse, O. & Weigand, J.J. 2022. Origin of morphology change and effect of crystallization time and Si/Al ratio during synthesis of zeolite ZSM-5. *ChemCatChem* 14(3): e202101248. https://doi.org/10.1002/cctc.202101248

Kowalska-Kuś, J., Held, A., Nowińska, K. & Góra-Marek, K. 2024. LTA zeolites as catalysts for transesterification of glycerol with dimethyl carbonate. *Fuel* 362: 130757. https://doi.org/10.1016/j.fuel.2023.130757

Kulkarni, S.B., Shiralkar, V.P., Kotasthane, A.N. & Borade, R.B. 1982. Studies in the synthesis of ZSM-5 zeolites. *Zeolites* 2(4): 313-318.

Lamnatou, C., Cristofari, C. & Chemisana, D. 2024. Renewable energy sources as a catalyst for energy transition: Technological innovations and an example of the energy transition in France. *Renewable Energy* 221: 119600. https://doi.org/10.1016/j.renene.2023.119600

Li, T., Krumeich, F., Chen, M., Ma, Z. & Van Bokhoven, J.A. 2020. Defining aluminum-zoning during synthesis of ZSM-5 zeolites. *Physical Chemistry Chemical Physics* 22(2): 734-739. https://doi.org/10.1039/c9cp05423e

Li, X., Han, S., Guan, D., Jiang, N., Xu, J. & Park, S.E. 2021. Rapid direct synthesis of nano-H-ZSM-5 from leached illite via solid-like-state conversion-based crystallization. *Applied Clay Science* 203: 106028. https://doi.org/10.1016/j.clay.2021.106028

Liu, C., Gu, W., Kong, D. & Guo, H. 2014. The significant effects of the alkali-metal cations on ZSM-5 zeolite synthesis: From mechanism to morphology. *Microporous and Mesoporous Materials* 183: 30-36. https://doi.org/10.1016/j.micromeso.2013.08.037

Lønstad Bleken, B-T., Mino, L., Giordanino, F., Beato, P., Svelle, S., Lillerud, K.P. & Bordiga, S. 2013. Probing the surface of nanosheet H-ZSM-5 with FTIR spectroscopy. *Physical Chemistry Chemical Physics* 15(32): 13363-13370. https://doi.org/10.1039/c3cp51280k

Mao, Y., Cheng, J., Guo, H., Shao, Y., Qian, L. & Yang, W. 2023. Sulfamic acid–modified zeolitic imidazolate framework (ZIF-90) with synergetic lewis and brønsted acid sites for microalgal biodiesel production. *Fuel* 331(P2): 125795. https://doi.org/10.1016/j.fuel.2022.125795

Md Sahabat Hossain, Md. Aftab Ali Shaikh, Md. Farid Ahmed & Samina Ahmed. 2023. Synthesis and characterization of nano-crystallite triple superphosphate from waste *Pila globosa* shells for sustainable industrial production. *Materials Advances* 4(10): 2384-2391. https://doi.org/10.1039/d3ma00102d

Medeiros Vicentini-Polette, C., Rodolfo Ramos, P., Bernardo Gonçalves, C. & Lopes De Oliveira, A. 2021. Determination of free fatty acids in crude vegetable oil samples obtained by high-pressure processes. *Food Chemistry* 12: 100166. https://doi.org/10.1016/j.fochx.2021.100166

Mosharof Hossain, Nuzhat Muntaha, Lipiar Khan Mohammad Osman Goni, Mohammad Shah Jamal, Mohammad Abdul Gafur, Dipa Islam & Abu Naieum Muhammad Fakhruddin. 2021. Triglyceride conversion of waste frying oil up to 98.46% using low concentration K^+/CaO catalysts derived from eggshells. *ACS Omega* 6(51): 35679-35691. https://doi.org/10.1021/acsomega.1c05582

Modather F. Hussein, Ahmed O. Abo El Naga, Mohamed El Saied, Mahmoud M. AbuBaker, Seham A. Shaban & Fathy Y. El Kady. 2021. Potato peel waste-derived carbon-based solid acid for the esterification of oleic acid to biodiesel. *Environmental Technology and Innovation* 21: 101355. https://doi.org/10.1016/j.eti.2021.101355

Nermein Mostafa Marzouk, Ahmed O. Abo El Naga, Sherif A. Younis, Seham A. Shaban, Abdel Monem El Torgoman & Fathy Y. El Kady. 2021. Process optimization of biodiesel production via esterification of oleic acid using sulfonated hierarchical mesoporous ZSM-5 as an efficient heterogeneous catalyst. *Journal of Environmental Chemical Engineering* 9(2): 105035. https://doi.org/10.1016/j.jece.2021.105035

Novita Andarini, Tanti Haryati, Suwardiyanto Suwardiyanto & Yudi Aris Sulistiyo. 2022. Synthesis of zeolite Y from lapindo mud with the comparative variation of the weight of NaOH/Mud and molar SiO_2/Al_2O_3. *Indonesian Chimica Letters* 1(1): 8-12. https://doi.org/10.19184/icl.v1i1.5

Pirzadi, Z. & Meshkani, F. 2022. From glycerol production to its value-added uses: A critical review. *Fuel* 329: 125044. https://doi.org/10.1016/j.fuel.2022.125044

Ponce, S., Gangotena, P.A., Anthony, C., Rodriguez, Y., Bazani, H.A.G., Keller, M.H., Souza, B.S., Vizuete, K., Debut, A. & Mora, J.R. 2024. Aluminum-based catalysts prepared in the presence of pectin for low-energy biodiesel production. *Fuel* 361: 130691. https://doi.org/10.1016/j.fuel.2023.130691

Praveena, V., Martin, L.J., Matijošius, J., Aloui, F., Pugazhendhi, A. & Varuvel, E.G. 2024. A systematic review on biofuel production and utilization from algae and waste feedstocks - A circular economy approach. *Renewable and Sustainable Energy Reviews* 192: 114178. https://doi.org/10.1016/j.rser.2023.114178

Prodinger, S., Berdiell, I.C., Cordero-Lanzac, T., Bygdnes, O.R., Solemsli, B.G., Kvande, K., Arstad, B., Beato, P., Olsbye, U. & Svelle, S. 2023. Cation-induced speciation of port-size during mordenite zeolite synthesis. *Journal of Materials Chemistry A* 11: 21884-21894.

Qurrota A'yuni, Ardhana Rahmayanti, Hartati Hartati, Purkan Purkan, Riki Subagyo, Nihayatur Rohmah, Luthfiyah Rifdah Itsnaini & Medya Ayunda Fitri. 2023. Synthesis and characterization of silica gel from lapindo volcanic mud with ethanol as a cosolvent for desiccant applications. *RSC Advances* 13(4): 2692-2699. https://doi.org/10.1039/d2ra07891k

Reber, M.J. & Brühwiler, D. 2015. Bimodal mesoporous silica with bottleneck pores. *Dalton Transactions* 44(41): 17960-17967. https://doi.org/10.1039/c5dt03082j

Rezayan, A. & Taghizadeh, M. 2018. Synthesis of magnetic mesoporous nanocrystalline KOH/ZSM-5-Fe_3O_4 for biodiesel production: Process optimization and kinetics study. *Process Safety and Environmental Protection* 117: 711-721. https://doi.org/10.1016/j.psep.2018.06.020

Ribeiro, F.C.P., Santos, J.L., Araujo, R.O., Santos, V.O., Chaar, J.S., Tenório, J.A.S. & de Souza, L.K.C. 2024. Sustainable catalysts for esterification: Sulfonated carbon spheres from biomass waste using hydrothermal carbonization. *Renewable Energy* 220: 119653. https://doi.org/10.1016/j.renene.2023.119653

Sathish Kumar, R.K, Sasikumar, R. & Dhilipkumar, T. 2024. Generation, bio-composite production, and environmental considerations. *Journal of Cleaner Production* 435: 140536. https://doi.org/10.1016/j.jclepro.2023.140536

Schulze-Makuch, D., Haque, S., Beckles, D., Schmitt-Kopplin, P., Harir, M., Schneider, B., Stumpp, C. & Wagner, D. 2020. A chemical and microbial characterization of selected mud volcanoes in trinidad reveals pathogens introduced by surface water and rain water. *Science of the Total Environment* 707: 136087. https://doi.org/10.1016/j.scitotenv.2019.136087

Rajasree Shanmuganathan, N.D. Nguyen, Mysoon M. Al-Ansari, Ezhaveni Sathiyamoorthi, Jintae Lee & S.D. Priya. 2024. Identification of suitable catalyst among HZSM-5, HY and γ-Al_2O_3 to obtain upgraded pyrolysis oil with augmented liquid oil yield. *Environmental Research* 260: 119587. https://doi.org/10.1016/j.envres.2024.119587

Su, C-H. 2013. Recoverable and reusable hydrochloric acid used as a homogeneous catalyst for biodiesel production. *Applied Energy* 104: 503-509. https://doi.org/10.1016/j.apenergy.2012.11.026

Thommes, M. 2010. Physical adsorption characterization of nanoporous materials. *Chemie-Ingenieur-Technik* 82(7): 1059-1073. https://doi.org/10.1002/cite.201000064

Trisunaryanti, W., Triyono, Paramesti, C., Larasati, S., Santoso, N.R. & Fatmawati, D.A. 2020. Synthesis and characterization of Ni/NH_2/mesoporous silica catalyst from lapindo mud for hydrocracking of waste cooking oil into biofuel. *RASAYAN Journal of Chemistry* 13(3): 1386-1393.

Van Poecke, A., Tabari, H. & Hellinckx, P. 2024. Unveiling the backbone of the renewable energy forecasting process: Exploring direct and indirect methods and their applications. *Energy Reports* 11: 544-557. https://doi.org/10.1016/j.egyr.2023.12.031

Wan Nur Aifa Wan Azahar, Mastura Bujang, Ramadhansyah Putra Jaya, Mohd Rosli Hainin, Azman Mohamed, Norzita Ngadi & Dewi Sri Jayanti. 2016. The potential of waste cooking oil as bio-asphalt for alternative binder - An overview. *Jurnal Teknologi* 78(4): 111-116. https://doi.org/10.11113/jt.v78.8007

Wang, H., Shen, B., Chen, X., Xiong, H., Wang, H., Song, W., Cui, C., Wei, F. & Qian, W. 2022. Modulating inherent lewis acidity at the intergrowth interface of mortise-tenon zeolite catalyst. *Nature Communications* 13: 2924. https://doi.org/10.1038/s41467-022-30538-7

Wang, Z., Jiang, X., Pan, M. & Shi, Y. 2020. Nano-scale pore structure and its multi-fractal characteristics of tight sandstone by N_2 adsorption/desorption analyses: A case study of shihezi formation from the sulige gas filed, Ordos Basin, China. *Minerals* 10(4): 377. https://doi.org/10.3390/min10040377

Weckhuysen, B.M. & Wachs, I.E. 2001. Catalysis by supported metal oxides. In *Handbook of Surfaces and Interfaces of Materials*, Vol. 1., edited by Nalwa, H.S. Massachusetts: Academic Press. pp. 613-648.

Wu, Q., Shu, Q., Guo, W. & Xing, X. 2024. Preparation of Brönsted-Lewis dual acidic catalyst Ce-HPW-F and its simultaneous catalytic esterification and transesterification of oleic acid and castor oil with methanol to synthesize biodiesel. *Fuel* 361: 130668. https://doi.org/10.1016/j.fuel.2023.130668

Xu, L., Zhang, J., Ding, J., Liu, T., Shi, G., Li, X., Dang, W., Cheng, Y. & Guo, R. 2020. Pore structure and fractal characteristics of different shale lithofacies in the dalong formation in the western area of the lower Yangtze platform. *Minerals* 10(1): 72. https://doi.org/10.3390/min10010072

Yadav, N., Yadav, G. & Ahmaruzzaman, M. 2023. Fabrication of surface-modified dual waste-derived biochar for biodiesel production by microwave-assisted esterification of oleic acid: Optimization, kinetics, and mechanistic studies. *Renewable Energy* 218: 119308. https://doi.org/10.1016/j.renene.2023.119308

Yang, J., Cong, W.J., Zhu, Z., Miao, Z-D., Wang, Y.T., Nelles, M. & Fang, Z. 2023. Microwave-assisted one-step production of biodiesel from waste cooking oil by magnetic bifunctional SrO–ZnO/MOF catalyst. *Journal of Cleaner Production* 395: 136182. https://doi.org/10.1016/j.jclepro.2023.136182

Ye, H., Shi, J., Wu, Y., Yuan, Y., Gan, L., Wu, Y., Xie, H., Pugazhendhi, A. & Xia, C. 2024. Research progress of nano-catalysts in the catalytic conversion of biomass to biofuels: Synthesis and application. *Fuel* 356: 129594. https://doi.org/10.1016/j.fuel.2023.129594

Zhang, P., Li, S. & Zhang, C. 2019. Solvent-free synthesis of nano-cancrinite from rice husk ash. *Biomass Conversion and Biorefinery* 9(3): 641-649. https://doi.org/10.1007/s13399-019-00375-8

Zhang, Q., Zhang, Y., Deng, T., Wei, F., Jin, J. & Ma, P. 2019. Sustainable production of biodiesel over heterogeneous acid catalysts. In *Biomass, Biofuels, Biochemicals: Recent Advances in Development of Platform Chemicals*, edited by Saravanamurugan, S., Pandey, A., Li, H. & Riisager, A. Elsevier. https://doi.org/10.1016/B978-0-444-64307-0.00016-0

*Corresponding author; email: hartati@fst.unair.ac.id